Editors' Suggestion

Is it possible to stabilize the 1144-phase pnictides with tri-valence cations?

B. Q. Song, Manh Cuong Nguyen, C. Z. Wang, P. C. Canfield, and K. M. Ho
Ames Laboratory, U.S. Department of Energy and Department of Physics and Astronomy, Iowa State University, Ames, Iowa 50011, USA

(Received 10 May 2018; revised manuscript received 12 August 2018; published 5 October 2018)

A lately discovered 1144 phase has generated significant interest for its high superconducting temperatures, disorder-free doping, and various chemical substitutions. However, it has only been found in iron arsenides ($ABFe_4As_4$), and cations are limited to +1 or +2 valence states (e.g., alkali metals, alkaline earth elements, and Eu). Whether more 1144 phases could be stabilized and whether intriguing properties exist are questions of general interest. In this work, we investigate 1144 iron and cobalt arsenides with tri-valence cations (La, Y, In, Tl, Sm, Gd). We study phase stability among other competing phases: 122 solution phase and phase decomposition. With La as the cation, we predict room-temperature stable 1144 structures: $LaAFe_4As_4$ (A = K, Rb, and Cs). Other La-contained 1144 structures tend to form solution phase. The solubility of La is estimated and compared with the experiment. By contrast, we do not find stable 1144 structures with Y as the cation. For In and Tl as cations, two 122-phase compounds are remarkably stable: $InCo_2As_2$ and $TlCo_2As_2$, which adds to our knowledge about the In(Tl)-Co-As phase diagram. Stable 1144 phases are found in $InKCo_4As_4$ and $InRbCo_4As_4$. With Sm and Gd as cations, 1144- or 122-phase iron arsenides are generally unstable. Among structures investigated, we recognize two critical factors for 1144-phase stability: size effect and charge balance, which yields a merging picture with the rule found in previous 1144 systems. Moreover, $LaAFe_4As_4$ (A = K, Rb, and Cs), $InCo_2As_2$, and $TlCo_2As_2$ are exhibiting semimetal features and a two-dimensional Fermi surface, similar to iron superconductors.

DOI: 10.1103/PhysRevMaterials.2.104802

I. INTRODUCTION

Iron pnictides superconductors (SC) [1–4] share a common crystalline feature of inserting cations between Fe-pnictogen skeleton layers, which is taken as an essential signature for SC. The 1144-phase iron arsenides ($ABFe_4As_4$) [6–8] belong to such a prototype [Fig. 1(a)] and show superconductivity at temperatures comparable to the 122 phase, which inspires great interest in searching for SC in this phase [6–19].

The 1144 phase $ABFe_4As_4$ (Fig. 1) has the same chemical composition as the 50%-doped 122 phase ($A_{0.5}B_{0.5}Fe_2As_2$), but different in the arrangement of the cation layers. In the 1144 phase, A and B atoms are occupying alternative cation layers, distinct from the random distribution in the 122 solution phase [5] [referred to as the 122(s) phase in this work]. The ordered cation arrangement leads to a lower crystalline symmetry, which is employed to generate novel spin textures (e.g., Hedgehog spin vertex) [8]. The 1144 phase has often been compared with the 122 phase in both experiments [6,7] and theory models [20].

The 1144 phase and the 122(s) phase compete with each other in forming crystals [6]. The stability of particular A-B cation combinations in 1144-phase iron arsenides depends on two primary factors: charge balance and size effects. Charge balance means the favorable A-B combination is alkali metal (IA group) with alkaline earth (IIA group), leading to an effective valence state of +1.5 for cations. Note that it is the charge situation of cations, instead of transition metals that accounts for the charge balance in this context. On the other hand, IA + IA or IIA + IIA lead to unstable 1144 phases [21]. The size effect is characterized by two descriptors: the mismatch in tetragonal lattice constants Δa and Δc [21] (or Δc could be replaced with the mismatch of atomic size Δr [6]). The 1144 phase is stabilized with a large $|\Delta c|$ and small $|\Delta a|$. Thus far, the rule developed by [6,21] works well for iron arsenides and seems promising to be generalized to a broad range of systems (e.g., Fe phosphides) [21].

So far, 1144-phase compounds with cations of IA and IIA group elements [6–8,22], as well as Eu [10,11,23,24], have been synthesized. Attempts in synthesizing new 1144 compounds with La has recently been made [9,13,25], but whether La-contained 1144 structures exist is still unclear. The primary challenge arises from the fact that La is a tri-valence cation and charge balance conditions are not satisfied. In this work, we try to address a general question: Is it possible to build tri-valence cations into the 1144 structures? We investigate six tri-valence elements: Y, La, In, Tl, Sm, and Gd. They can be classified into three groups. The first group includes Y ($4d^15s^2$) and La ($5d^16s^2$), which are nonmagnetic and similar to IA or IIA elements regarding the atomic size and a low electronegativity about 1.0. The second group is In and Tl. Despite the similar electronic shell structure as IA and IIA elements, the electronegativity (e.g., In 1.78, Tl 1.62 based on the Pauling scale) is higher than IA or IIA (generally below 1.0). A higher electronegativity allows In (or Tl) to compete with Fe in forming chemical bonding with As. Consequently, a stable binary alloy InAs is generated, impeding the formation of Fe-As layers. The third group contains Sm and Gd, which live in the neighborhood of Eu in the periodic table (Eu can form stable 122 iron arsenides) and similar to Eu concerning the shell structure, electronegativity, and atomic size.

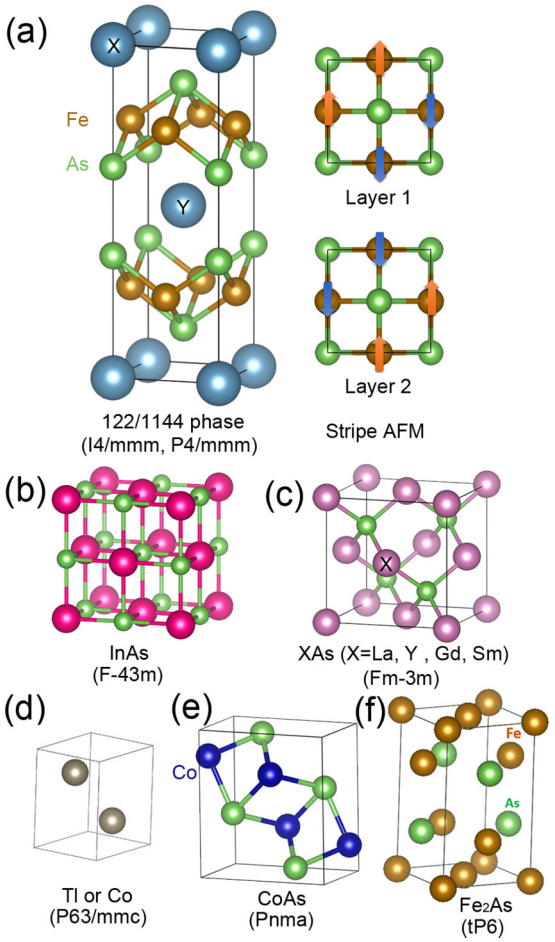

FIG. 1. Crystal structures involved in this work. (a) The 122/1144 phase. The 122 phase with X Y sites being occupied by the same cation. 1144 phase with X and Y being occupied by different cations. (b) InAs; (c) XAs (X = La, Y, Gd, Sm); (d) α phase of Tl or Co; (e) CoAs; (f) Fe_2As. The space group is labeled for each structure.

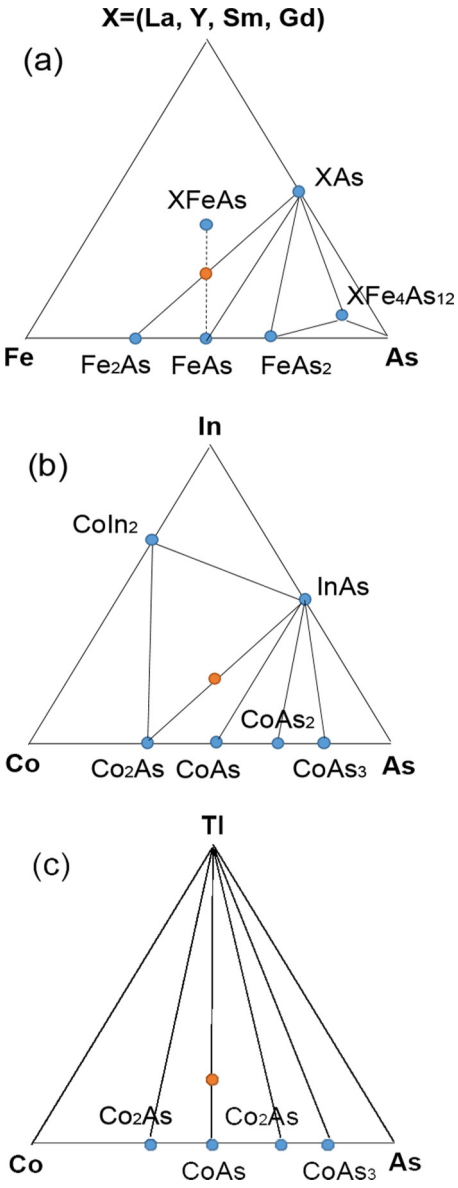

FIG. 2. The phase diagram of ternary alloys. (a) X-Fe-As (X = La, Y, Sm, and Gd); (b) In-Co-As; (c) Tl-Co-As. The known thermodynamically stable phase is denoted by blue dots on the graph. The 122 phase is designated as the orange dot.

The rest of the paper is organized as follows. Section II describes our methodology and calculation details. In each following section, one category of tri-valence elements will be discussed. In Sec. III, we discuss building La and Y into 1144 structures, explicitly focusing on $LaAFe_4As_4$ (A = Na, K, Rb, Cs, Ca, Sr, Ba). In Sec. IV, In and Tl are discussed. We propose stabilizing the 1144 structure by substituting Fe by Co. Thus we investigate $TlCo_2As_2$ and $InCo_2As_2$. We also study $TlACo_4As_4$ and $InACo_4As_4$ (A = K, Rb, Ca, Sr, Ba). Section V will discuss Sm and Gd cations in the 1144 phase.

II. METHODOLOGY AND CALCULATION DETAILS

The solution phase is higher in energy than phase decomposition, for which it is not the foremost competitor of the 1144 phase. Regarding entropy, the solution phase does not exist at zero temperature for the vanishing entropy (third law of thermodynamics). Hence, one is only obliged to consider the two-state competition: the 1144 phase and phase decomposition. Phase decomposition varies with systems, as shown in phase diagrams (Fig. 2).

At finite temperature, it involves the solution phase, which complicates the problem in two aspects. First, in estimating energy of the solution phase, one needs to consider all possible structural configurations [6,26–29]. The super cell modeling is apparently unfeasible, and we have adopted an approximation of the ideal solid solution:

$$E_{\mathrm{sol}} = xE_{A\mathrm{Fe2As2}} + (1-x)E_{B\mathrm{Fe2As2}}, \tag{1}$$

where E_{sol} is the energy of solution $A_xB_{1-x}Fe_2As_2$ and x is the concentration of A cations. Second, it involves several different entropies: configurational, vibrational, and electronic. It has demonstrated that the configurational entropy plays the most critical role [21]. Hence, we only consider configurational entropy under an ideal solid solution

approximation [30]:

$$S = -2k_B(x\log x + (1-x)\log(1-x)). \quad (2)$$

Then one is enabled to estimate the critical transition temperature of 1144-122(s) phases, as well as the La solubility at a given temperature. Note that, as an alternative approach, virtual crystal approximation (VCA) [31] could be used to investigate the electronic properties (e.g., band structures, density of states) of the solution phase. But reliable calculation also requires comparison with experiment data, for which its predicting power seems no more admirable than the ideal solution approximation.

All calculations of energy are based on density functional theory (DFT) and the Perdew Burke Ernzerhof (PBE) correlation functional [32], implemented by the Vienna *ab initio* simulation package (VASP) [33]. The projected augmented wave (PAW) pseudopotential method [34] is employed. The plane-wave energy cut is 400 eV. The k sampling has also been tested to ensure the convergence of energy. In calculating the enthalpy difference, we adopt spin-polarized calculation to account for the spin configurations. In calculating density of states (DOS) and band structures, we adopt a non-spin-polarized calculation, which has been commonly used in previous studies [35,36].

A single 1144 unit cell contains 10 atoms: one A, one B, four Fe, and four As atoms. A stripe antiferromagnetic (AFM) ordering [Fig. 1(a)] is adopted in our simulation of both 122 and 1144 phases. For the 122 phase, this has been substantiated by both experiments and calculations [37]. For the 1144 phase, it could display a different type of AFM [8], which is unfortunately beyond the predicting power of DFT. Thus, we adopt the low-energy spin configuration within the DFT framework. An enlarged $2 \times 2 \times 1$ supercell of $AB\mathrm{Fe_4As_4}$ is constructed to account for the magnetism. In Sec. IV we will consider cobalt arsenide, whose magnetism is not well known and more complicated. For example, $\mathrm{SrCo_2As_2}$ [38] and $\mathrm{BaCo_2As_2}$ [39] do not show any magnetic ordering down to 2 K. That probably indicates AFM and FM should be degenerate in energy. While $\mathrm{CaCo_2As_2}$ undergoes an AFM magnetic transition at 76 K and magnetic moment is aligned in the z axis [40], magnetism of $\mathrm{KCo_2As_2}$ and $\mathrm{RbCo_2As_2}$ is not well known. In addition, the recent study provides evidence of magnetic fluctuation of stripe-AFM and FM types in $\mathrm{SrCo_2As_2}$, despite the absence of magnetic ordering [41]. In our work, we adopt AFM for $\mathrm{CaCo_2As_2}$ and FM for the other four cobalt arsenides in calculating structural stability. In calculating band structures, we have adopted a nonmagnetic scenario.

III. La- AND Y-CONTAINED 1144 STRUCTURES

In this section, we will examine the stability of La- and Y-contained 1144 structures, as well as their electronic structures.

A. Phase stability at zero temperature

The phase diagram for La(Y)-Fe-As is presented in Fig. 2(a). Note that the 122 phase tends to decompose: $\mathrm{YFe_2As_2} \rightarrow \mathrm{YAs} + \mathrm{Fe_2As}$ and $\mathrm{LaFe_2As_2} \rightarrow \mathrm{LaAs} + \mathrm{Fe_2As}$. Thus one can define the enthalpy difference as

$$\Delta H^{122} = E_{\mathrm{LaFe2As2}} - (E_{\mathrm{LaAs}} + E_{\mathrm{Fe2As}}),$$
$$\Delta H^{122} = E_{\mathrm{YFe2As2}} - (E_{\mathrm{YAs}} + E_{\mathrm{Fe2As}}), \quad (3)$$

which are listed in the first row of Table I. We find positive ΔH for both $\mathrm{YFe_2As_2}$ and $\mathrm{LaFe_2As_2}$, which confirms the information given by the phase diagram. To prevent phase decomposition, we propose using a partner element (e.g., IA or IIA group elements), to form the La- or Y-contained 1144 phase. This idea is inspired by the author's earlier work [21],

TABLE I. The formation enthalpy of $\mathrm{LaFe_2As_2}$, $\mathrm{YFe_2As_2}$ (the first row in the table) and 1144 iron arsenides $\mathrm{La}A\mathrm{Fe_4As_4}$, $\mathrm{Y}A\mathrm{Fe_4As_4}$. The enthalpy of $\mathrm{LaFe_2As_2}$ and $\mathrm{YFe_2As_2}$ are measured with respect to phase decomposition: $\mathrm{Fe_2As} + M\mathrm{As}$ (M = La, Y). The formation enthalpies of La- and Y-contained 1144 structures are defined with respect to phase decomposition: $\mathrm{Fe_2As} + \mathrm{LaAs} + A\mathrm{Fe_2As_2}$ (A = Ca, Sr, Ba, Na, K, Rb, Cs). Positive ΔH favors phase decomposition. Note that the measuring point for ΔH is defined differently for 122 and 1144 phases.

	Lattice parameters (Å)	ΔH (meV/atom)		Lattice (Å)	ΔH (meV/atom)
La	$a = 3.8427$ $c = 11.9341$	19.54	Y	$a = 3.7737$ $c = 11.5686$	86.51
LaCa	$a = 3.843$ $c = 12.091$	6.73	YCa	$a = 3.820$ $c = 11.767$	51.13
LaSr	$a = 3.897$ $c = 12.210$	1.54	YSr	$a = 3.869$ $c = 11.919$	47.96
LaBa	$a = 3.943$ $c = 12.394$	0.67	YBa	$a = 3.928$ $c = 12.049$	41.11
LaNa	$a = 3.797$ $c = 12.599$	−0.39	YNa	$a = 3.737$ $c = 12.373$	30.92
LaK	$a = 3.828$ $c = 13.109$	−13.91	YK	$a = 3.813$ $c = 12.758$	17.81
LaRb	$a = 3.843$ $c = 13.386$	−17.22	YRb	$a = 3.820$ $c = 13.106$	16.03
LaCs	$a = 3.878$ $c = 13.628$	−18.28	YCs	$a = 3.866$ $c = 13.289$	12.81

which suggests that the favorable valence state of cations in forming the 1144 phase is +1.5. Thus, La^{3+} is accompanied with IA group elements to lower its valence state in forming the 1144 phase.

To test this idea, we study both IA elements (Na, K, Rb, Cs) and IIA elements (Ca, Sr, Ba). The ΔH of 1144 structures are defined as

$$\Delta H^{1144} = E_{\mathrm{LaAFe4As4}} - (E_{A\mathrm{Fe2As2}} + E_{\mathrm{LaAs}} + E_{\mathrm{Fe2As}}),$$
$$\Delta H^{1144} = E_{\mathrm{YAFe2As2}} - (E_{A\mathrm{Fe2As2}} + E_{\mathrm{YAs}} + E_{\mathrm{Fe2As}}). \quad (4)$$

The definition of ΔH for the 1144 phase is notably different from the 122 phase. Also note that we have precluded a metastable phase decomposition: $LaFe_2As_2 \rightarrow LaFeAs + FeAs$ [as the dashed line shown in Fig. 2(a)], which is 200 meV/atom higher in formation enthalpy.

The calculated ΔH are listed in Table I, indicating four stable 1144 compounds: $LaNaFe_4As_4$, $LaKFe_4As_4$, $LaRbFe_4As_4$, and $LaCsFe_4As_4$. By contrast, it proves to be unstable for all Y-contained 1144 compounds. In addition, two trends for ΔH are recognized. First, La + IA combinations are preferred in stabilizing the 1144 phase compared with La + IIA, which is consistent with the anticipation. Second, the stability of the 1144 phase is enhanced with an increased radius of the A atom. We plot the ΔH vs atomic radius of A in $LaAFe_4As_4$ and $YAFe_4As_4$ in Fig. 3. Evidently, ΔH keep decreasing as the radius of the cation is increased. The phase stability has been attributed to a rule about structural factors [6], and the rule is well fitted to experimental findings. However, the range of cation combinations in previous studies was confined to IA + IIA, wherein the charge balance effect is concealed and structural factors have thereby become outstanding.

B. Phase stability at finite temperature

At finite temperature, there exist three competing matter states: the 1144 phase, the phase decomposition ($AFe_2As_2 + LaAs + Fe_2As$), and the 122(s) phase. The free energy at a given temperature is

$$\Delta G = \Delta H - T\Delta S. \quad (5)$$

For simplicity, we only consider configurational entropy. Since the 1144 phase and phases produced by decomposition are entirely ordered, the configuration entropy is zero. On the other hand, the 122(s) phase has configuration entropy due to randomness, which is 0.012 meV/(atom K). Thus at high enough temperature, the 122(s) phase will eventually predominate owing to $-T\Delta S$. We can estimate the critical temperature, which makes $\Delta G = 0$. We find the following critical temperatures: 45 K for $LaNaFe_4As_4$, 1615 K for $LaKFe_4As_4$, 2000 K for $LaRbFe_4As_4$, and 2123 K for $LaCsFe_4As_4$. For an achievable 1144 phase, it requires the critical temperature to be comparable to the growth temperature, as the crystal is grown at 800–1000 K, then cooling down to room temperature [7]. Thus, La-Na will form the solution phase at room temperature, while other three cation combinations (LaK, LaRb, and LaCs) seem promising to form the 1144 phase. Note that recent attempts have been focused on cation combinations of La-Na [13,25], which leads to a solution phase.

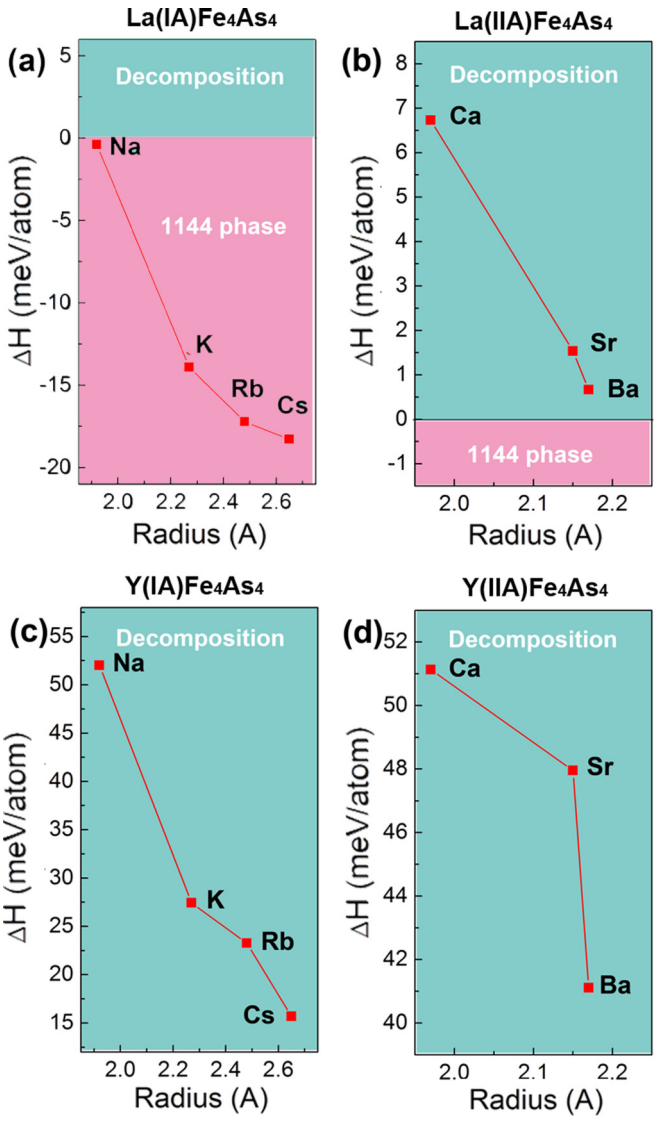

FIG. 3. ΔH dependence on atomic radius of cations in several La- and Y-contained 1144 structures. Positive ΔH favors phase decomposition, colored in blue, while negative ΔH favors 1144 phase, colored in red. Evidently, ΔH decreases as the cation radius increases. Thus, the 1144 phase is better stabilized with larger cations.

For those unstable combinations ($LaAFe_4As_4$, A = Ca, Sr, and Ba), the system will undergo phase decomposition. However, at finite temperature, a certain amount of La will inevitably dissolve into the AFe_2As_2 and form a solution phase $(La_xA_{1-x})Fe_2As_2$. Since x would be nonzero at finite temperature, there is no sharp boundary between the pure 122 phase and the 122(s) phase. The pure 122 phase observed in the experiment should be regarded as a doped 122 phase with extremely low concentration.

To estimate the maximum solubility x at a given temperature, we consider a La-rich environment: $(La_yA_{1-y}Fe_2As_2)$, $(y > x)$. Energy drives the system to decompose into ordered phases:

$$La_yA_{1-y}Fe_2As_2 \rightarrow (1-y)AFe_2As_2 + yLaAs + yFe_2As. \quad (6)$$

On the other hand, with the effect of entropy, it leads to

$$\mathrm{La}_y A_{1-y}\mathrm{Fe}_2\mathrm{As}_2 \rightarrow \frac{1-y}{1-x}\mathrm{La}_x A_{1-x}\mathrm{Fe}_2\mathrm{As}_2 + \frac{y-x}{1-x}\mathrm{LaAs} + \frac{y-x}{1-x}\mathrm{Fe}_2\mathrm{As}, \quad (7)$$

where $\mathrm{La}_x A_{1-x}\mathrm{Fe}_2\mathrm{As}_2$ is the solution phase with the maximum amount of La dissolved. Evidently, the enthalpy favors decomposition (6), while the entropy favors decomposition (7). Thus, the two decompositions are competing and will eventually reach a balance. At the balance point, we have $\Delta G = 0$, where ΔG is the free energy difference between the two decompositions (6) and (7). The enthalpy part of ΔG is estimated by DFT with a supercell model. In computing enthalpy of the solution phase $\mathrm{La}_x A_{1-x}\mathrm{Fe}_2\mathrm{As}_2$, we adopt the ideal solution approximation, as defined in Eq. (1). The entropy part of ΔG is estimated with Eq. (2)

Then the maximum solubility x will be solved by

$$-2k_B T(x\log x + (1-x)\log(1-x)) = 10x(\Delta H), \quad (8)$$

The factor 10 arises from there being 10 atoms in each unit cell. ΔH is the formation enthalpy of $\mathrm{LaFe}_2\mathrm{As}_2$ or $\mathrm{YFe}_2\mathrm{As}_2$ (Table I). By setting $T = 300\,\mathrm{K}$, we find the solubility x is 20% for La and 10^{-9} for Y. It indicates that $\mathrm{La}A\mathrm{Fe}_2\mathrm{As}_2$ (A = Ca, Sr, Ba) will be La doped to a considerable amount, while Y is not dopable and pure $A\mathrm{Fe}_2\mathrm{As}_2$ will be obtained at room temperature. Note that for systems of $\Delta H > 0$ the maximum doping concentration only depends on the formation enthalpy of $\mathrm{LaFe}_2\mathrm{As}_2$, independent of the solvent, i.e., insensitive to cation atom A in $A\mathrm{Fe}_2\mathrm{As}_2$ (A = Ca, Sr, Ba).

Based on the analysis above, we argue that the 1144-phase $\mathrm{La}A\mathrm{Fe}_4\mathrm{As}_4$ (A = K, Rb,Cs) will maintain at temperatures 1000 K or even higher. $\mathrm{LaNaFe}_4\mathrm{As}_4$ will favor the 1144 phase below 45 K and will transform into the 122(s) phase (about 50% La concentration) at higher temperatures. For A = Ca, Sr, Ba, we will get the 122(s) phase of 20% La concentrations.

Recently, it finds that La-Ca will lead to a La-doped $\mathrm{CaFe}_2\mathrm{As}_2$ up to 20% [42]. For La-Na, it leads to 40% doping [13,25], which is lower but close to our prediction 50%. In addition, preliminary attempts have been made on La-contained 1144 structures [9].

C. Electronic structures

For the intimate relation, the 1144 phase is usually compared with the 122 phase. Several key features have been identified for the 122 iron arsenides. For example, it exhibits concentric hole-type FS at the Γ point in the Brillouin zone (B.Z.) and electronic elliptical FS around M points (The M point in primitive tetragonal B.Z. corresponds to the X point in the body-centered-tetragonal B.Z. [37]). The Fe 3-d orbitals mainly contribute to the density of states near the Fermi level. The $4p$ orbitals of As are 2–6 eV below the Fermi surface (FS) due to the strong As-Fe interaction [35,36]. Therefore, it is believed that Fe $3d$ bands are responsible for superconductivity. It also shows that iron-based SC exhibit quasi-two-dimensional FS [35,36]. Thus, a two-dimensional (2D)

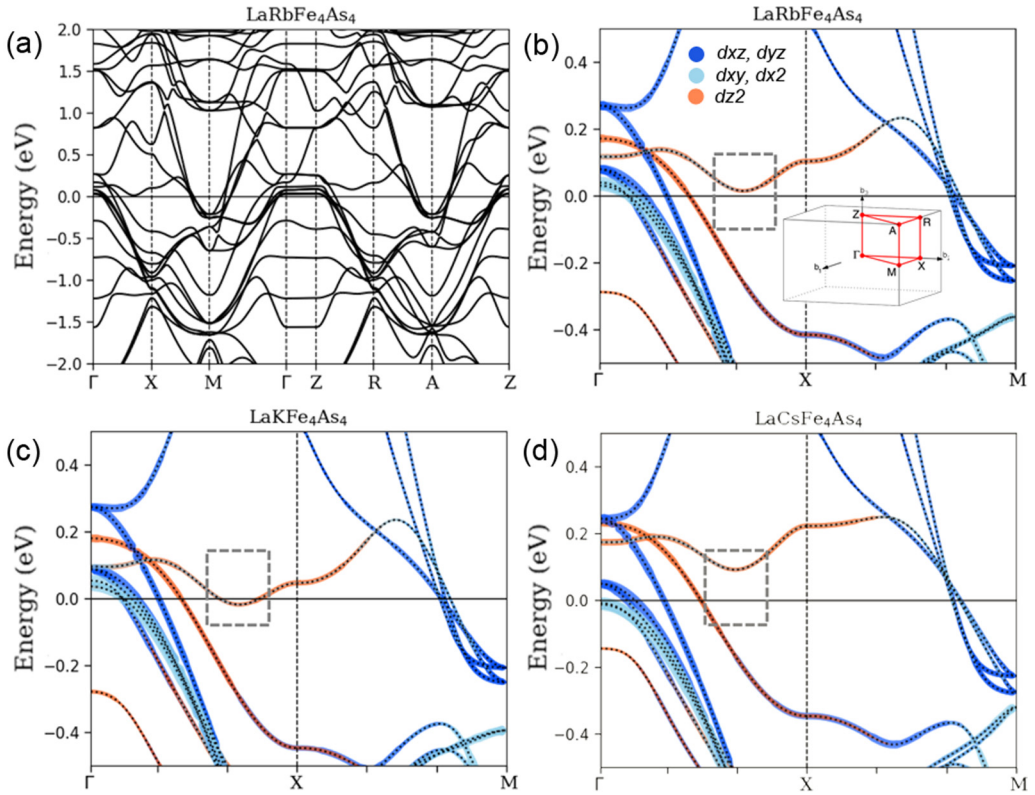

FIG. 4. (a) Band structure of $\mathrm{LaRbFe}_4\mathrm{As}_4$. (b) Zoom-in of (a), in which the inset shows the primitive tetragonal B.Z. In (a) and (b), there are six bands crossing the Fermi level near the Γ point and four bands near the M point. (c) and (d) The band structures of $\mathrm{LaKFe}_4\mathrm{As}_4$ and $\mathrm{LaCsFe}_4\mathrm{As}_4$.

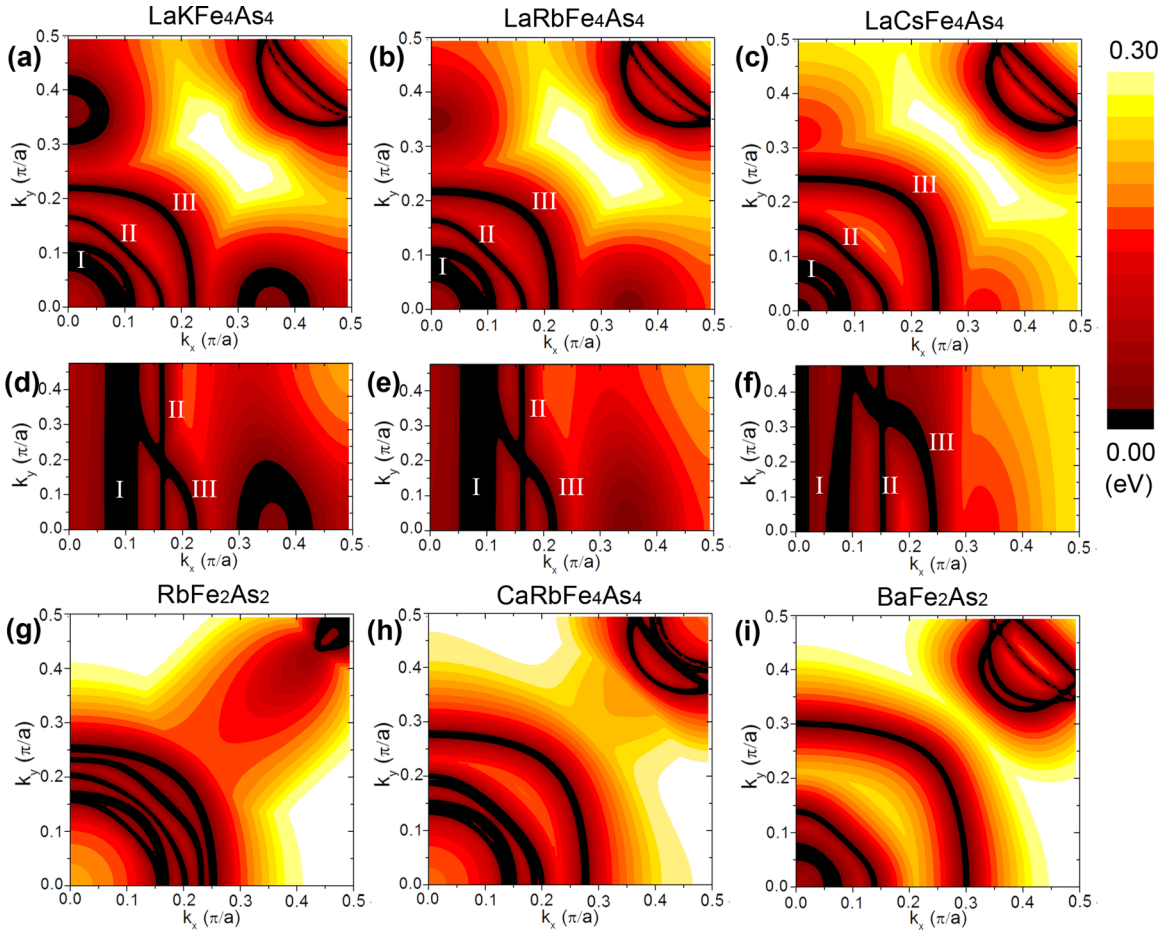

FIG. 5. (a)–(c) Fermi surface (shown as the black color) in the $k_z = 0$ plane for $LaKFe_4As_4$, $LaRbFe_4As_4$, and $LaCsFe_4As_4$. The color scale represents the energy difference between the nearest band to the Fermi level. (d)–(f) Fermi surface of the three systems in the $k_x = 0$ plane. (g)–(i) Fermi surface of $RbFe_2As_2$, $CaRbFe_4As_4$, and $BaFe_2As_2$ in the $k_z = 0$ plane. The color bar is interpolated linearly in energy.

Hamiltonian model is proposed as an attempt to understand SC physics [43].

The band structures of the three most stable $LaAFe_4As_4$ (A = K, Rb, and Cs) are calculated. We try to address whether the 2D FS retains as La being introduced and, also, whether it is still a semimetal—hole pocket at Γ and electron pocket at M, which is believed critical for superconductivity. Note that even isovalent substitution might essentially change the topology of FS. For instance, the electron-type FS does not exist in KFe_2As_2 [44], in contrast with $RbFe_2As_2$ [45] and $CsFe_2As_2$ [46].

The band structures of the three 1144 structures are plotted in Fig. 4. The band structures all feature a hole-type FS near the Γ point in B.Z. and an electron-type FS near the M point. From the zoom-in band [Fig. 4(b)], six bands are found crossing the Fermi level near the Γ point, and four bands near the M point. At the Γ point, the six bands can be grouped into three sets, which behave differently as varying the A atom in $LaAFe_4As_4$. The inner four bands are labeled as I. The single-fold band in the middle is labeled as II. The largest and outermost band is designated by III (Fig. 5). In the k_z direction, bands I and II feature weak dispersion, thus can be considered 2D [Figs. 5(d)—5(f)]. By contrast, the FS of band III shrinks along the z direction, and eventually merges into the FS of band I. In the k_x-k_y plane, the three systems have FS of similar shapes, but of different sizes. The FS due to band I in the $k_z = 0$ plane will shrink as the radius of cation is increased. In particular, two FS sheets in $LaCsFe_4As_4$ almost shrink to vanishing. Band II generally remains unaltered when the cations are varied, while the FS of band III will expand its size as the radius of cations is increased. On the other hand, the electron-type FS near the M point is scarcely affected by the cation species. Therefore, cation substitution will mainly influence the FS near the Γ point.

Unique features are identified in $LaKFe_4As_4$: an additional band is crossing the Fermi level between the Γ and X points, resulting in another sheet of FS [Fig. 4(c)]. The additional FS is like a hollow bubble and will disappear along the k_z direction [Figs. 5(a) and 5(d)].

For $LaAFe_4As_4$ (A = Cs Rb K), each unit cell contains two cation atoms and transfers a total of four electrons from cations to the Fe-As layer. In this regard, it should exhibit similar electronic structures as $BaFe_2As_2$, which is transferring the same amount of charges. In Fig. 5(i), we present the FS of $BaFe_2As_2$. We find $BaFe_2As_2$ has four sheets of hole-type FS at the Γ point and four sheets of electron-type FS at the

TABLE II. Lattice constants (calculated values) and formation enthalpy of In- and Tl-contained 122 compounds. The last column is the valence state of In or Tl in 122 compounds.

	Lattice parameters (Å)	ΔH (meV/atom)	Cation valence
$InFe_2As_2$	$a = 3.724$	3.12	+1
	$c = 13.806$		
$TlFe_2As_2$	$a = 3.755$	137.55	+1
	$c = 13.986$		
$InCo_2As_2$	$a = 3.769$	−84.89	+1
	$c = 13.354$		
$TlCo_2As_2$	$a = 3.780$	−267.94	+1
	$c = 13.675$		

M point, while $LaRbFe_4As_4$ has six FS sheets at Γ and four sheets at M as mentioned above. The difference is caused by two bands in $BaFe_2As_2$ that become filled as energy being suppressed.

$CaRbFe_4As_4$ has one fewer electron transferred to the Fe-As layer [47]. We compare $LaRbFe_4As_4$ with $CaRbFe_4As_4$. Since $LaRbFe_4As_4$ has one more electron, the Fermi energy is expected to shift higher in energy. Our calculation is consistent with expectation, showing a larger FS at the M point and smaller FS at the Γ point. Thus, FS size changes in $CaRbFe_4As_4$ and $LaRbFe_4As_4$ can be qualitatively understood by a rigid shift of Fermi level. Then we examine $RbFe_2As_2$, which has two fewer valence electrons compared with $LaRbFe_4As_4$. $RbFe_2As_2$ has a larger hole-type FS at Γ and small FS at the M point, which is also consistent with the rigid shift of FS. In addition, $RbFe_2As_2$ have six FS sheets at Γ and four sheets at the M point, the same as $LaRbFe_4As_4$.

IV. MAIN GROUP ELEMENTS (IIIA)

In this section, we study In- and Tl-contained 122 or 1144 structures as well as their electronic structures.

A. Phase stability

Like La and Y, In and Tl do not favor 122 iron arsenides. Our earlier calculation concludes that enthalpy favors the decomposition of $InFe_2As_2$ into InAs and Fe_2As [21]. For $TlFe_2As_2$, it follows a different decomposition: $TlFe_2As_2 \rightarrow Tl + 2(FeAs)$. Binary alloys of Tl-As are unstable and they will decompose into their elementals [Figs. 2(b) and 2(c)]. Based on that, the enthalpy difference ΔH is defined as

$$\Delta H^{122} = E_{\mathrm{TlFe2As2}} - (E_{\mathrm{Tl}} + 2E_{\mathrm{FeAs}}),$$
$$\Delta H^{122} = E_{\mathrm{InFe2As2}} - (E_{\mathrm{InAs}} + E_{\mathrm{Fe2As}}). \quad (9)$$

The ΔH of $TlFe_2As_2$ and $InFe_2As_2$ are listed in Table II. Note that for both Tl and In, the 122 iron arsenide is unstable. This is seemingly another evidence that the +3 cations do not favor 122-type iron arsenides. However, orbital occupancy suggests that In or Tl in this environment only lose one of the three valence electrons to the Fe-As layers, forming In^+ or Tl^+ (Table II). The higher electronegativity of In and Tl is responsible for such partial loss of valence electrons. The unstable 122 phase should be relevant to the metastable +1 cations. Thus, it is essential to stabilize the +1 valence state in order to form the 122 phase.

The solution we propose is to inject extra electrons into Fe-As layers to adjust the chemical potential, such that Fe-As layers will be less attractive to the valence electrons of In. Then, forming the +1 valence state will become more favorable in energy. For this purpose, we substitute all Fe by Co, i.e., $InCo_2As_2$ and $TlCo_2As_2$. Based on the phase diagram Fig. 2(b), the enthalpy difference of 122 $InCo_2As_2$ is defined as

$$\Delta H^{122} = E_{\mathrm{InCo2As2}} - (E_{\mathrm{Co}} + E_{\mathrm{InAs}} + E_{\mathrm{CoAs}}). \quad (10)$$

Note that Tl undergoes a different decomposition [Fig. 2(c)]. The formation enthalpy of $TlCo_2As_2$ is thereby defined as

$$\Delta H^{122} = E_{\mathrm{TlCo2As2}} - (E_{\mathrm{Tl}} + 2E_{\mathrm{CoAs}}). \quad (11)$$

To estimate the energy, one needs to determine the magnetic ordering in the Co-As layer. Cobalt arsenides exhibit complex magnetism. For instance, $SrCo_2As_2$ [38] and $BaCo_2As_2$ [39] do not show any magnetic ordering down to 2 K. By contrast, $CaCo_2As_2$ undergoes a AFM phase transition at 76 K [40]. Moreover, these systems feature complex magnetic fluctuations. For example, $SrCo_2As_2$ even with a paramagnetic magnetism at $T = 5$ K, reveals AFM spin fluctuations, similar to the AFM ordering found in 122 iron arsenide [41].

In our DFT study, we have considered six spin configurations [48] and find that the energies of these configurations are close. This is consistent with the paramagnetic ground state as found in the experiment. We adopt the following magnetic ordering in our calculation: FM for $BaCo_2As_2$ and $SrCo_2As_2$; AFM for $CaCo_2As_2$ (AFM means interlayer AFM, in-plane Co is still FM); for $InCo_2As_2$, $TlCo_2As_2$, and KCo_2As_2, different spin configurations all converge to a nonmagnetic ground state, neither AFM nor FM. The magnetic configuration for the binary alloy has been studied in the experiment. For example, FeAs is showing an AFM spiral magnetic ordering [49]. Fe_2As also shows an AFM magnetic ordering [50].

The enthalpies of $InCo_2As_2$ and $TlCo_2As_2$ are listed in Table II. It indicates that the stability of the 122 phase is remarkably enhanced when Fe is replaced by Co. As far as we know, there have not been many reports on the ternary alloy of In-Co-As or Tl-Co-As [Figs. 2(b) and 2(c)]. Nevertheless, the present study is supposed to modify the original phase diagram. Besides, $InCo_2As_2$ and $TlCo_2As_2$ can be regarded as unusual 122 structures in terms of the chemical composition. It is known that the 122 phase has generally followed such a formula: a nonmetal element (e.g., P, As, Se) with electronegativity 2.0–2.5 plus an active metal with an electronegativity <1.0 (e.g., alkali metals or alkaline earth) and a transition metal with electronegativity >1.5. With such chemical composition, pnictogen and transition metals will form the layered skeleton, wherein As or P will form covalent bonds with transition metals rather than perfect ion bonds. The active metals inserted between the skeleton layer will lose all their valence electrons, injecting charges into skeleton layers. Most 122 structures (e.g., $CaFe_2As_2$ and KFe_2As_2) belong to this type. However, in the case of $InCo_2As_2$ and $TlCo_2As_2$, the

TABLE III. The lattice constants (calculated values) and enthalpy differences for 1144-phase structures InACo$_4$As$_4$ and TlACo$_4$As$_4$.

	Lattice parameters (Å)	ΔH (meV/atom)		Lattice (Å)	ΔH (meV/atom)
InCa	$a = 3.822$	11.76	TlCa	$a = 3.834$	11.57
	$c = 12.441$			$c = 12.565$	
InSr	$a = 3.815$	13.17	TlSr	$a = 3.861$	12.41
	$c = 12.887$			$c = 12.847$	
InBa	$a = 3.838$	13.11	TlBa	$a = 3.849$	12.69
	$c = 13.157$			$c = 13.316$	
InK	$a = 3.769$	−2.28	TlK	$a = 3.784$	0.03
	$c = 13.567$			$c = 13.742$	
InRb	$a = 3.788$	−1.05	TlRb	$a = 3.799$	0.08
	$c = 13.759$			$c = 14.007$	

cation atoms have high electronegativity >1.5. In this regard, $InCo_2As_2$ and $TlCo_2As_2$ have unusual chemical compositions and suggest a different strategy of searching for new 122 compounds.

Note that 122 compounds ACo_2As_2 (A = Ca, Sr, Ba, K, Rb, etc.) also exist. It is interesting to examine whether 1144 cobalt arsenides can be stabilized by combining two 122 phases. The enthalpy for cobalt is defined as

$$\Delta H^{1144} = E_{\mathrm{In}A\mathrm{Co4As4}} - (E_{\mathrm{InCo2As2}} + E_{A\mathrm{Co2As2}}),$$
$$\Delta H^{1144} = E_{\mathrm{In}A\mathrm{Co4As4}} - (E_{\mathrm{TlCo2As2}} + E_{A\mathrm{Co2As2}}). \quad (12)$$

The enthalpy of 1144 structures is listed in Table III. We find two systems might form 1144 structures: $InKCo_4As_4$ and $InRbCo_4As_4$. We also notice in terms of stabilizing the 1144 structures combinations of In or Tl with IA are generally better than combining with IIA elements; smaller A atoms are better than larger ones.

B. Electronic structure

The density of states (DOS) of $InCo_2As_2$ and $TlCo_2As_2$ are plotted in Figs. 6(a) and 6(b). The states near the Fermi level are mainly contributed by d orbitals of Co. The In(Tl)'s s orbitals lie deep below Fermi energy. For In, the s orbitals

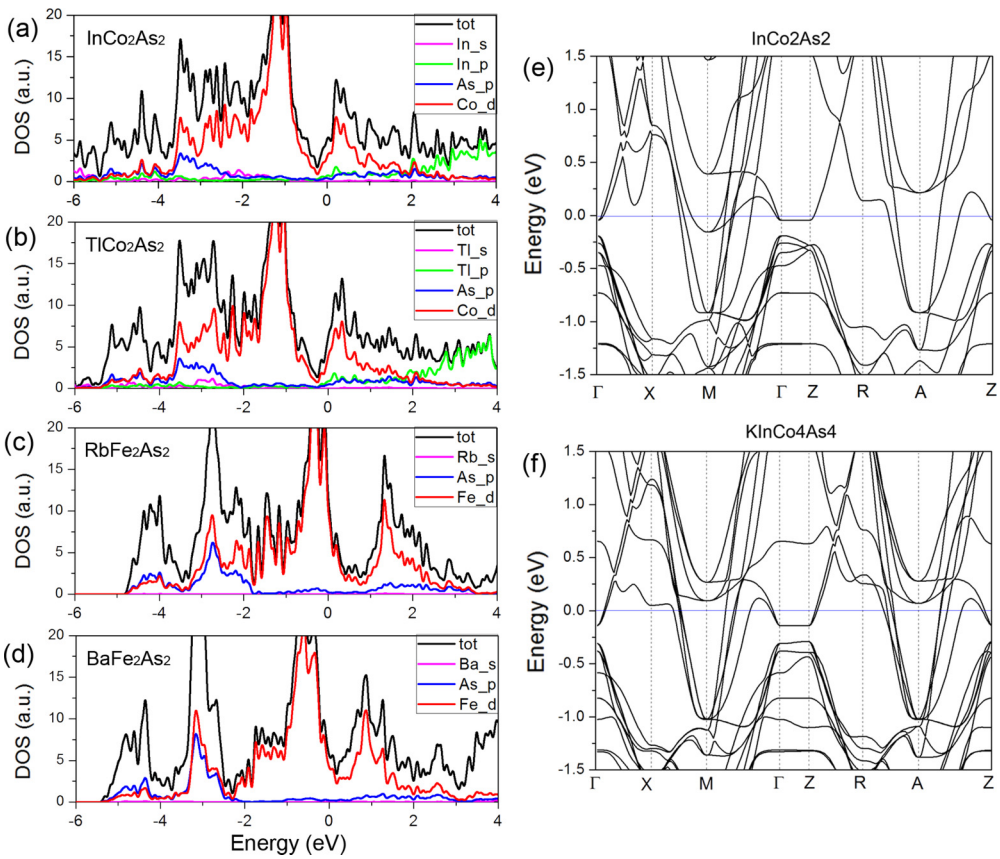

FIG. 6. DOS and projected DOS of (a) $InCo_2As_2$, (b) $TlCo_2As_2$, (c) $RbFe_2As_2$, and (d) $BaFe_2As_2$. The band structure of (e) $InCo_2As_2$ and (f) $KInCo_4As_4$.

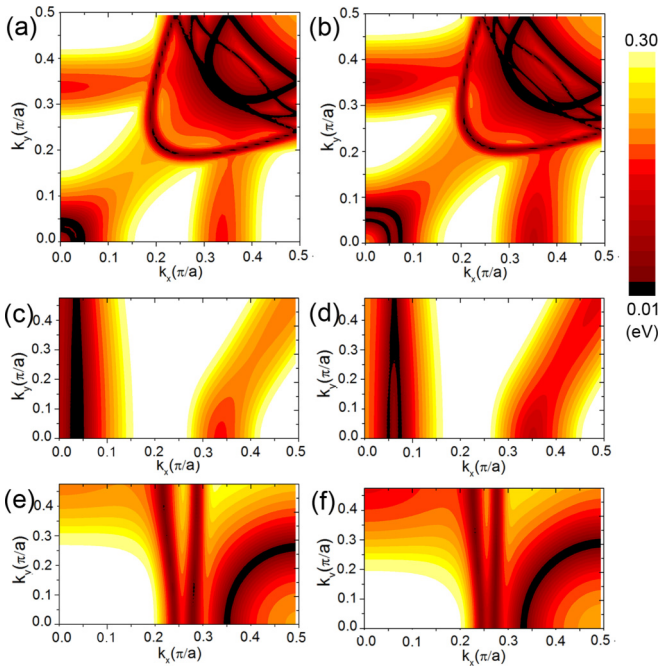

FIG. 7. The Fermi surface of $InCo_2As_2$ [(a), (c), and (e)] and $TlCo_2As_2$ [(b), (d), and (f)] in the $k_z = 0$, $k_y = 0$, and $k_y = 0.5$ plane. The color scale represents the energy difference between the nearest band to Fermi level. In calculating these Co arsenides, we have adopted the same supercell of $2 \times 2 \times 1$ as Fe arsenides.

are peaked around −2.0 and −6.0 eV, while for Tl the peaks are around −3.0 and −4.5 eV. Compared with iron, cobalt will introduce extra charges. Thus the Fermi level of $InCo_2As_2$ should be shifted higher, compared with $RbFe_2As_2$ and $BaFe_2As_2$ [Figs. 6(c) and 6(d)]. The calculated DOS is consistent with such expectation. Figures 6(a) and 6(b) clearly show that the FS is located above the valley between the conduction bands and valence bands. While the FS in Figs. 6(c) and 6(d) is located below it. Consequently, the DOS at the Fermi level for $InCo_2As_2$ and $TlCo_2As_2$ is smaller than that of $RbFe_2As_2$ and $BaFe_2As_2$. In addition, for In(Tl)Co_2As_2, the p orbital of In(Tl) also contributes to the states at FS. By contrast, in iron arsenides, those states are almost solely contributed by the Fe 3d orbital.

The band structures of $InCo_2As_2$ are displayed in Fig. 6(e), which features electron pockets around the Γ and M points. Two bands are crossing the Fermi level at the Γ point and six bands (three double-degeneracy bands) at the M point, resulting in multiple FS sheets. The $TlCo_2As_2$ has almost the identical band structure as $InCo_2As_2$. The FS of the two compounds are plotted in Fig. 7. Literally, it shows that a small FS sheet exists around the Γ point and another set of elliptical FS sheets exists around the M point. The FS around the Γ point consists of two sheets. Near the M point there are six FS sheets, which will generate three sets of double-fold degeneracy on the boundary of B.Z. Figures 7(c) and 7(d) show that the FS sheets around the Γ point are pretty two-dimensional through the B.Z. At the M point, four of the six FS sheets can be regarded two-dimensional. On the other hand, the inner FS sheet is bubblelike and will disappear along the k_z direction. As expected, $InCo_2As_2$ and $TlCo_2As_2$ resemble band structures and FS topology, except the FS of Tl near the Γ point is slightly larger. It is known that the 122 cobalt arsenide $SrCo_2As_2$ is showing complicated FS topology and not showing SC in the observing temperature range [38]. The absence of superconductivity could be rationalized by the distinct FS topology. Regarding this, $InCo_2As_2$ is more similar to iron arsenide SC in band structures, and could serve as a testing ground for the role of FS played in SC. The band structure of $InKCo_4As_4$ is given in Fig. 6(f). $InRbCo_4As_4$ has very a similar band structure as $InKCo_4As_4$, thus it is not shown here.

TABLE IV. Lattice constants and enthalpy difference for 122-phase structures $SmFe_2As_2$ and $GdFe_2As_2$ (the first row in table) and 1144-phase structures SmAFe$_4$As$_4$ and GdAFe$_4$As$_4$.

	Lattice parameters (Å)	ΔH (meV/atom)		Lattice (Å)	ΔH (meV/atom)
Sm	$a = 3.780$	66.82	Gd	$a = 3.774$	83.24
	$c = 17.775$			$c = 11.639$	
SmCa	$a = 3.811$	35.60	GdCa	$a = 3.778$	49.08
	$c = 11.953$			$c = 11.899$	
SmSr	$a = 3.853$	31.65	GdSr	$a = 3.822$	41.71
	$c = 12.116$			$c = 12.213$	
SmBa	$a = 3.910$	24.90	GdBa	$a = 3.883$	37.67
	$c = 12.322$			$c = 12.310$	
SmNa	$a = 3.722$	41.58	GdNa	$a = 3.737$	42.68
	$c = 12.503$			$c = 12.374$	
SmK	$a = 3.802$	13.50	GdK	$a = 3.790$	21.51
	$c = 13.004$			$c = 13.004$	
SmRb	$a = 3.859$	1.77	GdRb	$a = 3.848$	9.31
	$c = 13.040$			$c = 12.951$	
SmCs	$a = 3.882$	−1.00	GdCs	$a = 3.876$	4.71
	$c = 13.315$			$c = 13.184$	

V. Sm- AND Gd-CONTAINED 1144 STRUCTURE

Sm and Gd do not form stable 122-phase iron arsenides, as shown in the phase diagram [Fig. 2(a)]. Instead, they will decompose: $SmFe_2As_2 \rightarrow SmAs + Fe_2As$ and $GdFe_2As_2 \rightarrow GdAs + Fe_2As$. Thus, we define the enthalpy measured to the energy of phase decomposition:

$$\Delta H^{122} = E_{SmFe2As2} - (E_{SmAs} + E_{Fe2As}),$$
$$\Delta H^{122} = E_{GdFe2As2} - (E_{GdAs} + E_{Fe2As}). \quad (13)$$

Compared with La and Y, Gd and Sm have a half-filled f orbital and thus are magnetic. In treating Sm and Gd, we have employed PAW potentials that build the f electron into the core, which is a routine way to cope with the inabilities of the present DFT functional to describe the localized orbitals.

The formation enthalpies of $SmFe_2As_2$ and $GdFe_2As_2$ are presented in Table IV. Both $GdFe_2As_2$ and $SmFe_2As_2$ are showing positive ΔH (Table IV), which suggests phase decomposition. Physically, this is due to the fact that Sm and Gd tend to form +3 cations, violating the rule of charge balance. The enthalpy differences are 66.82 meV/atom for Sm and 83.24 meV/atom for Gd. These values are greater than La but less than Y.

Since the electronegativity of Sm and Gd is close to that of La and Y, we use a similar strategy to stabilize the 1144 phase. We examine $SmAFe_4As_4$ and $GdAFe_4As_4$ (A = IA and IIA elements). The formation enthalpy of 1144 phases is defined as

$$\Delta H^{1144} = E_{SmAFe4As4} - (E_{AFe2As2} + E_{SmAs} + E_{Fe2As}),$$
$$\Delta H^{1144} = E_{GdAFe4As4} - (E_{AFe2As2} + E_{GdAs} + E_{Fe2As}). \quad (14)$$

We list the enthalpy differences in Table IV, among which only $SmCsFe_4As_4$ shows negative enthalpy. It seems that the 1144 phase can hardly be stabilized. However, we still notice that group IA elements are generally better in stabilizing the 1144 phase than group IIA elements. Therefore, charge balance is still taking effect. In addition, as the radius of the cation increases, the stability of 1144 improves. This is consistent with the general trends we already found in La- and Y-contained 1144 structures.

VI. CONCLUSION

In this work, we have discussed which A-B combinations can stabilize the 1144 phase, with the peculiar focus on trivalence cations (La, Y, In, Tl, Sm, and Gd). Even though La does not support 122 iron arsenides, three La-contained 1144 compounds are found stable at room temperatures: $LaAFe_4As_4$ (A = K, Rb, and Cs). For In and Tl, iron arsenides ($InFe_2As_2$ and $TlFe_2As_2$) prove to be unstable due to the metastable cation In^+ and Tl^+. Replacing Fe with Co will substantially enhance the 122 phase: $InCo_2As_2$ and $TlCo_2As_2$, which renews our traditional knowledge about the In(Tl)-Co-As phase diagram. By contrast, Y, Sm, and Gd do not practically support any 122 or 1144 phases.

TABLE V. Summary of stable 1144- and 122-phase structures that contain tri-valence elements, as well as some relevant structures. The column Γ and M show the number of bands crossing the Fermi level as well as the FS type (particle or hole). The rightmost column shows the valence state of cations in particular compounds.

	Γ	M	ΔH (meV/atom)	Critical T (K)	
$LaCsFe_4As_4$	6 (h)	4 (p)	−18.28	2123	La^{3+}, Cs^{1+}
$LaRbFe_4As_4$	6 (h)	4 (p)	−17.22	2000	La^{3+}, Rb^{1+}
$LaKFe_4As_4$	6 (h)	4 (p)	−13.91	1615	La^{3+}, K^{1+}
$RbFe_2As_2$	6 (h)	4 (p)			Rb^{1+}
$CaRbFe_4As_4$	5 (h)	4 (p)	−15.70	700 [21]	Ca^{2+}, Rb^{1+}
$BaFe_2As_2$	4 (h)	4 (p)			Ba^{2+}
$InCo_2As_2$	2 (p)	6 (p)			In^{1+}
$TlCo_2As_2$	2 (p)	6 (p)			Tl^{1+}

Stability of these 1144 structures is not random but following specific rules: (1) alkali metals are preferable in stabilizing the 1144 phase to alkaline earth elements, which is due to the fact that alkali metal plus La (forming an effective +2 valence state) is close to the optimal state +1.5 for forming 1144-phase Fe arsenides; (2) atoms of the larger size will better support the 1144 phase than smaller ones (e.g., Cs is better than K). Physically, the rules are consequences of two factors: the charge balance and the size effect. In this work, we examine the effects of the two factors in various Fe arsenides and Co arsenides. It seems to apply generically to 1144 structures.

A characteristic of iron SC is semimetal features with electron and hole pockets. The 1144 phase $LaAFe_4As_4$ (A = K, Rb, and Cs) and 122 phase ACo_2As_2 (A = In, Tl) both exhibit semimetal features and two-dimensional Fermi surfaces. An intriguing question is whether superconductivity forms in these systems. Critical information about band structures and phase stability is summarized in Table V.

The 1144 phase provides a structural prototype, and by chemical substitutions one is able to obtain various such compounds. Our work suggests two approaches for substitutions: first, changing the cation combination; second, substituting transition metals. Combining the two dimensions of variation, there exists a vast reservoir of 1144 systems to be explored.

ACKNOWLEDGMENTS

We wish to acknowledge the very helpful discussion with Sergey Budko, Tai Kong, William Meier, and Mingyu Xu. This work was supported by the U.S. Department of Energy (DOE), Office of Science, Basic Energy Sciences, Materials Science and Engineering Division, including the grant of computer time at the National Energy Research Scientific Computing Center (NERSC) in Berkeley, CA. The research was performed at Ames Laboratory, which is operated for the U.S. DOE by Iowa State University under Contract No. DE-AC02-07CH11358.

[1] Y. Kamihara, T. Watanabe, M. Hirano, and H. Hosono, J. Am. Chem. Soc. **130**, 3296 (2008).
[2] J. W. Lynn and P. Dai, Physica C **469**, 469 (2009).
[3] D. N. Basovand and A. V. Chubukov, Nat. Phys. **7**, 272 (2011).

[4] Z. Bukowski, S. Weyeneth, R. Puzniak, J. Karpinski, and B. Batlogg, Physica C **470**, S328 (2010).

[5] E. Z. Kurmaev, J. A. McLeod, A. Buling, N. A. Skorikov, A. Moewes, M. Neumann, M. A. Korotin, Yu. A. Izyumov, N. Ni, and P. C. Canfield, Phys. Rev. B **80**, 054508 (2009).

[6] A. Iyo, K. Kawashima, T. Kinjo, T. Nishio, S. Ishida, H. Fujihisa, Y. Gotoh, K. Kihou, H. Eisaki, and Y. Yoshida, J. Am. Chem. Soc. **138**, 3410 (2016).

[7] W. R. Meier, T. Kong, U. S. Kaluarachchi, V. Taufour, N. H. Jo, G. Drachuck, A. E. Bohmer, S. M. Saunders, A. Sapkota, A. Kreyssig, M. A. Tanatar, R. Prozorov, A. I. Goldman, F. F. Balakirev, Alex Gurevich, S. L. Budko, and P. C. Canfield, Phys. Rev. B **94**, 064501 (2016).

[8] W. R. Meier, Q. P. Ding, A. Kreyssig, S. L. Bud'ko, A. Sapkota, K. Kothapalli, V. Borisov, R. Valenti, C. D. Batista, P. P. Orth, R. M. Fernandes, A. I. Goldman, Y. Furukawa, A. E. Bohmer, and P. C. Canfield, npj Quantum Materials **3**, 5 (2018).

[9] K. Kawashima, S. Ishida, H. Fujihisa, Y. Gotoh, K. Kihou, Y. Yoshida, H. Eisaki, H. Ogino, and A. Iyo, J. Phys. Chem. Lett. **9**, 868 (2018).

[10] Y. Liu, Y.-B. Liu, Q. Chen, Z.-T. Tang, W.-H. Jiao, Q. Tao, Z.-A. Xu, and G.-H. Cao, Science Bulletin **61**, 1213 (2016).

[11] Y. Liu, Y. B. Liu, Z. T. Tang, H. Jiang, Z. C. Wang, A. Ablimit, W. H. Jiao, Q. Tao, C. M. Feng, Z. A. Xu, and G. H. Cao, Phys. Rev. B **93**, 214503 (2016).

[12] K. Kawashima, T. Kinjo, T. Nishio, S. Ishida, H. Fujihisa, Y. Gotoh, K. Kihou, H. Eisaki, Y. Yoshida, and A. Iyo, J. Phys. Soc. Jpn. **85**, 064710 (2016).

[13] A. Iyo, K. Kawashima, S. Ishida, H. Fujihisa, Y. Gotoh, H. Eisaki, and Y. Yoshida, J. Am. Chem. Soc. **140**, 369 (2018).

[14] T. Xie, D. Gong, W. Zhang, Y. Gu, Z. Husges, D. Chen, Y. Liu, L. Hao, S. Meng, Z. Lu, S. Li, and H. Luo, Supercond. Sci. Technol. **30** 095002 (2017).

[15] W. R. Meier, T. Kong, S. L. Bud'ko, and P. C. Canfield, Phys. Rev. Mater. **1**, 013401 (2017).

[16] P. K. Biswas, A. Iyo, Y. Yoshida, H. Eisaki, K. Kawashima, and A. D. Hillier, Phys. Rev. B **95**, 140505(R) (2017).

[17] K. Cho, A. Fente, S. Teknowijoyo, M. A. Tanatar, K. R. Joshi, N. M. Nusran, T. Kong, W. R. Meier, U. Kaluarachchi, I. Guillamon, H. Suderow, S. L. Bud'ko, P. C. Canfield, and R. Prozorov, Phys. Rev. B **95**, 100502(R) (2017).

[18] R. Yang, Y. Dai, B. Xu, W. Zhang, Z. Qiu, Q. Sui, C. C. Homes, and X. Qiu, Phys. Rev. B **95**, 064506 (2017).

[19] D. Mou, T. Kong, W. R. Meier, F. Lochner, L. L. Wang, Q. Lin, Y. Wu, S. L. Bud'ko, I. Eremin, D. D. Johnson, P. C. Canfield, and A. Kaminski, Phys. Rev. Lett. **117**, 277001 (2016).

[20] F. Lochner, F. Ahn, T. Hickel, and I. Eremin, Phys. Rev. B **96**, 094521 (2017).

[21] B. Q. Song, M. C. Nguyen, C. Z. Wang, and K. M. Ho, Phys. Rev. B **97**, 094105 (2018).

[22] S. A. J. Kimber, A. Kreyssig, Y. Zhang, H. O. Jeschke, R. Valentí, F. Yokaichiya, E. Colombier, J. Yan, T. C. Hansen, T. Chatterji, R. J. McQueeney, P. C. Canfield, A. I. Goldman, and D. N. Argyriou, Nat. Mater. **8**, 471 (2009).

[23] H. S. Jeevan, D. Kasinathan, H. Rosner, and P. Gegenwart, Phys. Rev. B **83**, 054511 (2011).

[24] Y. Tokiwa, S. H. Hubner, O. Beck, H. S. Jeevan, and P. Gegenwart, Phys. Rev. B **86**, 220505 (2012).

[25] J. Q. Yan, S. Nandi, B. Saparov, P. Cermak, Y. Xiao, Y. Su, W. T. Jin, A. Schneidewind, T. Bruckel, R. W. McCallum, T. A. Lograsso, B. C. Sales, and D. G. Mandrus, Phys. Rev. B **91**, 024501 (2015).

[26] K. Zhao, Q. Q. Liu, X. C. Wang, Z. Deng, Y. X. Lv, J. L. Zhu, F. Y. Li, and C. Q. Jin, J. Phys.: Condens. Matter **22**, 222203 (2010).

[27] D. M. Wang, X. C. Shangguan, J. B. He, L. X. Zhao, Y. J. Long, P. P. Wang, and L. Wang, J. Supercond. Novel Magn. **26**, 2121 (2013).

[28] K. Sasmal, B. Lv, B. Lorenz, A. M. Guloy, F. Chen, Y. Y. Xue, and C. W. Chu, Phys. Rev. Lett. **101**, 107007 (2008).

[29] G. Wu, H. Chen, T. Wu, Y. L. Xie, Y. J. Yan, R. H. Liu, X. F. Wang, J. J. Ying, and X. H. Chen, J. Phys.: Condens. Matter **20**, 422201 (2008).

[30] D. R. Gaskell, *Introduction to the Thermodynamics of Materials*, 5th ed. (Taylor and Francis, Philadelphia, 2008).

[31] S. de Gironcoli, P. Giannozzi, and S. Baroni, Phys. Rev. Lett. **66**, 2116 (1991).

[32] J. P. Perdew, K. Burke, and M. Ernzerhof, Phys. Rev. Lett. **78**, 1396 (1997).

[33] G. Kresse and J. Furthmüller, Comput. Mater. Sci. **6**, 15 (1996).

[34] P. E. Blochl, Phys. Rev. B **50**, 17953 (1994).

[35] D. J. Singh and M. H. Du, Phys. Rev. Lett. **100**, 237003 (2008).

[36] I. I. Mazin and J. Schmalian, Physica C **469**, 614 (2009).

[37] D. C. Johnston, Adv. Phys. **59**, 803 (2010).

[38] A. Pandey, D. G. Quirinale, W. Jayasekara, A. Sapkota, M. G. Kim, R. S. Dhaka, Y. Lee, T. W. Heitmann, P. W. Stephens, V. Ogloblichev, A. Kreyssig, R. J. McQueeney, A. I. Goldman, Adam Kaminski, B. N. Harmon, Y. Furukawa, and D. C. Johnston, Phys. Rev. B **88**, 014526 (2013).

[39] A. S. Sefat, D. J. Singh, R. Jin, M. A. McGuire, B. C. Sales, and D. Mandrus, Phys. Rev. B **79**, 024512 (2009).

[40] B. Cheng, B. F. Hu, R. H. Yuan, T. Dong, A. F. Fang, Z. G. Chen, G. Xu, Y. G. Shi, P. Zheng, J. L. Luo, and N. L. Wang, Phys. Rev. B **85**, 144426 (2012).

[41] P. Wiecki, V. Ogloblichev, A. Pandey, D. C. Johnston, and Y. Furukawa, Phys. Rev. B **91**, 220406(R) (2015).

[42] Z. Xing, T. J. Huffman, P. Xu, A. J. Hollingshad, D. J. Brooker, N. E. Penthorn, M. M. Qazilbash, S. R. Saha, T. Drye, C. Roncaioli, and J. Paglione, Phys. Rev. B **94**, 064514 (2016).

[43] A. B. Vorontsov, M. G. Vavilov, and A. V. Chubukov, Phys. Rev. B **81**, 174538 (2010).

[44] S. Maiti, M. M. Korshunov, and A. V. Chubukov, Phys. Rev. B **85**, 014511 (2012).

[45] M. Aftabuzzaman and A. K. M. A. Islam, Physica C **470**, 202 (2010).

[46] S. Kong, D. Y. Liu, S. T. Cui, S. L. Ju, A. F. Wang, X. G. Luo, L. J. Zou, X. H. Chen, G. B. Zhang, and Z. Sun, Phys. Rev. B **92**, 184512 (2015).

[47] X. Shi and G. Wang, J. Phys. Soc. Jpn. **85**, 124714 (2016).

[48] Consider three types of in-plane magnetic ordering: FM and stripe-AFM $(0, \pi)$, AFM with (π, π). Two types of interplane magnetic ordering FM and AFM for each of the three types of in-plane ordering. Thus in all we consider six spin configurations.

[49] N. Kazama and H. Watanabe, J. Phys. Soc. Jpn. **30**, 578 (1971).

[50] H. Katsuraki and K. Suzuki, J. Appl. Phys. **36**, 1094 (1965).